

# Non-localities and Fermi motion corrections in $K^-$ atoms

C. García-Recio<sup>a)</sup>, J. Nieves<sup>a)</sup>,  
E. Oset<sup>b)</sup> and A. Ramos<sup>c)</sup>

a) Departamento de Física Moderna,  
Universidad de Granada, E-18071 Granada, Spain

b) Departamento de Física Teórica and IFIC,  
Centro Mixto Universidad de Valencia-CSIC,  
Institutos de Investigación de Paterna,  
Aptdo. Correos 22085, 46071 Valencia, Spain

c) Departament d'Estructura i Constituents de la Matèria,  
Universitat de Barcelona, 08028 Barcelona, Spain

November 11, 2018

## Abstract

We evaluate the p-wave  $K^-N$  amplitudes from the chiral Lagrangians and from there construct the p-wave part of the  $K^-$  nucleus optical potential plus a small s-wave part induced from the elementary p-wave amplitude and the nuclear Fermi motion. Simultaneously, the momentum and energy dependence of the s-wave optical potential, previously developed, are taken into account and shown to generate a small p-wave correction to the optical potential. All the corrections considered are small compared to the leading s-wave potential, and lead to changes in the shifts and widths which are smaller than the experimental errors. A thorough study of the threshold region and low densities is conducted, revealing mathematical problems for which a physical solution is given.

PACS: 13.75.Jz; 21.30.Fe; 21.65.+f; 25.80.Nv; 36.10.Gv

[Key Words] Kaonic atom, Non-localities in optical potential, Chiral unitary model

# 1 Introduction

The problem of kaonic atoms has attracted considerable attention along the years [1–9] and has regained interest recently due to the new perspective that the use of chiral Lagrangians has brought to the problem of the kaon interaction with a nuclear medium [10–13]. The need to obtain accurate results for the kaon selfenergy in a nuclear medium in view of the possibility to get kaon condensates in neutron-proton stars [14–16] has also added a renewed interest in the subject. Similarly, the interpretation [17,18] of the enhancement of the  $K^-$  yields in heavy ion reactions [19,20] relies on the value of the  $K^-$  selfenergy in the nuclear medium. One of the characteristics of the  $\bar{K}N$  interaction at low energies is the strong dominance of the s-wave amplitude, and the  $\bar{K}N$  cross section to different channels can be very well described with only s-waves up to momenta of the order of 200 MeV or more [21–25].

The dominance of the s-wave in the elementary interaction has been the justification for using traditionally s-wave  $\bar{K}$  nucleus optical potentials [1–9], by means of which good agreement with data can be obtained. This is in contrast with the situation in pionic atoms, since the relative small contribution of the s-wave part of the potential, together with a sizeable p-wave part, make this latter contribution quite important in the interpretation of the pionic atom data [26–28].

Theoretical evaluations of the optical potential for a particle in a nucleus usually start from the impulse approximation, or  $t\rho$  form of the potential, with  $t$  the elementary scattering amplitude of the particle with the nucleons averaged over isospin and the Fermi motion of the nucleons. Yet, it is known that the explicit consideration of the Fermi motion leads to corrections to this result. Certainly there are other higher order corrections in the density from mechanisms involving many nucleons, which one can systematically tackle using many body techniques [28], but even at the level of one single scattering the explicit consideration of Fermi motion brings corrections to the optical potential beyond the  $t\rho$  approach. A detailed study of these correction terms for the case of pionic atoms was done in [29], where it was found that the s-wave elementary amplitude induces a p-wave term in the optical potential and, similarly, the p-wave elementary amplitude induces an s-wave term. Yet, these corrections are small compared to the original impulse approximation and even small compared to the  $\rho^2$  terms which account for pion absorption.

The aims of the present paper are to investigate the nonlocal effects induced from the s-wave part of the  $K^-$  nucleus optical potential and also to evaluate the p-wave part of it. Firstly, we begin from the part of the potential evaluated from the s-wave  $K^-N$  interaction in [13] and derive from there the nonlocal corrections originated from the  $\omega$  and  $k$  dependence of this potential. These non-local terms were evaluated in [30] and there they were found to be large and quantitatively important in the analysis of the spectra of kaonic atoms. We also evaluate the part of the potential originating from the elementary p-wave  $K^-N$  interaction and deduce from there the p-wave term of the optical potential plus an induced s-wave part due to the Fermi motion of the nucleons.

We shall see that all these corrections are rather small and do not appreciably change the results obtained from the s-wave part of the potential alone.

One important finding is that, in order to properly evaluate these corrections, one must pay a special attention to the region of low densities. Consequently we discuss in detail the problems that one faces implementing the low density limit around a threshold, particularly in the derivatives of the optical potential.

Finally, we study the effects of the inclusion of the  $\Sigma^* - h$  excitation in the self-consistent calculation of the s-wave  $K^-$  potential. We find that, though best-fits of better quality can be obtained, this new theoretical potential leads to an overall acceptable description of the measured shifts and widths.

## 2 Brief summary of the $\bar{K}N$ and $\bar{K}$ nucleus interactions

For the elementary  $\bar{K}N$  interaction we follow the chiral unitary model of [24]. This work follows closely the steps of [23], where the usefulness of combining unitarity in coupled channels with the chiral Lagrangian was made manifest, but uses an enlarged basis of coupled channels. The inclusion of all the channels formed by the octets of the pseudoscalar mesons and stable baryons made it possible to obtain good solutions in [24] by means of only the lowest order chiral Lagrangian and a suitable cut off to regularize the loop integrals. On the other hand, in [23] the effect of the unopened channels was accounted for by including higher order terms in the chiral Lagrangian.

The  $K^-N$   $t$  matrix,  $t_{ij}$ , is obtained in [24] through the iteration of the Lagrangian in a coupled channel Bethe–Salpeter equation.

The  $K^-$  selfenergy is evaluated in detail in ref. [13] for nuclear matter by means of the integral

$$\Pi(k, \rho) = 2 \sum_N \int \frac{d^3p}{(2\pi)^3} n(\vec{p}, \rho) t_{K^-N}^{(m)}(k, \vec{p}, \rho), \quad (1)$$

where  $N$  stands for protons or neutrons and  $t^{(m)}$  is the  $K^-N$  scattering matrix in the nuclear medium with density  $\rho$ . In Eq. (1),  $n(\vec{p}, \rho)$  denotes the occupation probability of momentum states in the Fermi sea in the nuclear medium at finite density  $\rho$ . Only the s-wave amplitude is considered in this evaluation. In section 5 we shall work out the contribution from the p-wave interaction.

The  $t^{(m)}$  matrix is evaluated from the Bethe–Salpeter equation, but modifications are done in the meson and baryon propagators of the loops to incorporate the medium effects. The states allowed in the loops are  $\bar{K}N$ ,  $\pi\Sigma$ ,  $\pi\Lambda$ ,  $\eta\Sigma$ ,  $\eta\Lambda$ ,  $K\Xi$ .

The medium modifications implemented are the following:

1) Pauli blocking in the nucleon propagators. This effect was proved to be very important in [10,11]. Indeed, forcing the intermediate nucleon states to be on top of a Fermi sea costs more energy, and the net effect is a shift to higher energies of both the real and imaginary parts of the  $K^-p$  amplitude which is dominated by the  $\Lambda(1405)$  resonance below threshold. The shift of the real part automatically produces an attractive  $K^-$  selfenergy already at very small densities.

2) However, if the  $K^-$  selfenergy acquires a negative value then it costs less energy to produce the  $\Lambda(1405)$  resonance hence producing a shift of the  $K^-p$  amplitude toward lower energies. A selfconsistent evaluation becomes then necessary as shown in [12], where it was found that the consideration of the  $K^-$  selfenergy together with Pauli blocking on the nucleons left the position of the  $\Lambda(1405)$  resonance basically unchanged. In [13] the  $K^-$  selfenergy is also considered and a selfconsistent evaluation is also done.

3) In addition to the former ingredients new effects are considered in [13], i.e. the pion selfenergy in the  $\pi\Sigma$ ,  $\pi\Lambda$  channels is also taken into account allowing the pions to excite  $ph$ ,  $\Delta h$  and  $2p2h$  components. Furthermore, the difference of binding between the nucleons or  $\Sigma$  and  $\Lambda$  hyperons is also incorporated.

The results obtained are qualitatively similar to those found in [12] except that the imaginary part of the  $K^-p$  amplitude becomes even wider and essentially flattens at full nuclear density  $\rho \sim \rho_0$ .

### 3 Nonlocal terms associated to the s-wave part of the potential

As described in the former section the optical potential for the  $K^-$  nucleus interaction was evaluated in nuclear matter as a function of the density in [13] and, in order to apply it to finite nuclei, the local density approach was used in [8], something justified for the s-wave potential as discussed in [28]. The  $K^-$  selfenergy obtained in [13] from the interaction of the  $K^-$  with protons and neutrons in symmetric nuclear matter has an explicit dependence on  $k^0 = \omega$  and  $\vec{k}$ , the energy and momentum of the antikaon. However, in order to solve the Klein–Gordon equation (KGE) to obtain energies and widths of the kaonic atoms in [8], the potential was evaluated at the  $K^-$  threshold ( $\omega = m_K, \vec{k} = 0$ ). In what follows we derive the corrections to the optical potential from the consideration of the explicit  $\omega$  and  $\vec{k}$  dependence of the kaon selfenergy in the nuclear medium.

We write the  $K^-$  selfenergy in nuclear matter,  $\Pi$ , as

$$\Pi(\omega, \vec{k}, \rho) = 2\omega V_{opt} = \Pi(m_K, 0, \rho) + b(\rho) \vec{k}^2 + c(\rho) (\omega - m_K) , \quad (2)$$

with

$$b(\rho) = \left. \frac{\partial \Pi}{\partial \vec{k}^2} \right|_{(\omega=m_K, \vec{k}=0)} , \quad c(\rho) = \left. \frac{\partial \Pi}{\partial \omega} \right|_{(\omega=m_K, \vec{k}=0)} , \quad (3)$$

where the second order corrections in  $\vec{k}^2$  and  $(\omega - m_K)$  have been neglected.

Once at this point the momentum  $\vec{k}$  is not defined for the bound  $K^-$  in the atom and instead it becomes an operator. In detailed studies of finite nuclei one can trace the origin of this operator and how it acts on the density-dependent functions of the potential or the kaonic wave function. For instance, in [28] one can see that the  $\vec{k}^2$  which appears in the

p-wave part of the  $\pi$ -nucleus optical potential evaluated in nuclear matter corresponds in the equivalent finite nucleus calculation to the combination

$$\vec{k}_{CM}^2 f(\rho) \rightarrow \frac{1}{(1 + \varepsilon)^2} \left[ -\vec{\nabla} f(\rho(\vec{r})) \vec{\nabla} + \frac{1}{2} \varepsilon \vec{\nabla}^2 f(\rho(\vec{r})) \right], \quad \varepsilon = \frac{m_\pi}{M_N}. \quad (4)$$

In the present case the evaluation of the  $K^-$  selfenergy in finite nuclei, with all the effects considered in [12, 13] plus the requirement of selfconsistency is a rather involved task, which would become advisable should these nonlocal effects be too big. Yet, as we shall see, the effects are small, smaller than present experimental uncertainties in the data, and thus the estimates which we shall perform here are sufficient to establish the relevance of these effects. One of the handicaps of having evaluated the selfenergy in infinite nuclear matter is that we do not know to which kind of  $\vec{\nabla} \vec{\nabla}$  operator will the factor  $\vec{k}^2$  correspond to. In order to estimate the size of the corrections and the uncertainties, we shall work with some different assumptions which are guided by the results obtained for pionic atoms in the translation from infinite matter to finite nuclei. The types of operators used for the  $b \vec{k}^2$  term of the  $K^-$ -selfenergy in Eq. (2) are shown below

$$\begin{aligned} \text{a) } b \vec{k}^2 &\rightarrow -\vec{\nabla} b \vec{\nabla} \\ \text{b) } b \vec{k}^2 &\rightarrow -\vec{\nabla} b \vec{\nabla} - \frac{1}{2} (\Delta b) \\ \text{c) } b \vec{k}^2 &\rightarrow -b \vec{\nabla}^2 \end{aligned} \quad (5)$$

The form a) is the Kisslinger type of interaction  $\vec{k} \cdot b \vec{k}$ , the form b) appears in [29] by using the Wigner transform of the symmetrized form  $(b \vec{k}^2 + \vec{k}^2 b)/2$ , the form c) allows the  $\vec{k}^2$  operator to act directly on the kaonic wave function, and thus has a special physical significance.

We can also adopt a different point of view and, since the results of Eq. (1) already come from using local approximations implicit in the use of a local Fermi sea, we can convert the nonlocal potential of  $\vec{k}^2$  into a local, but energy dependent, potential. The trade between nonlocal and local energy dependent potentials is a technique often used in many body theory [31]. It is based on the use of the Schrödinger equation (KGE in our case). The KGE is written here as

$$[-\vec{\nabla}^2 + \mu^2 + \Pi(r)] \phi(\vec{r}) = [\omega - V_C(r)]^2 \phi(\vec{r}). \quad (6)$$

where  $\mu$  is the kaon-nucleus reduced mass and  $V_C(r)$  is the Coulomb potential with a finite nuclear size and vacuum-polarization corrections.

In view of Eq. (6), and the fact that the meaning of  $\vec{k}^2$  in Eq. (2) is the kaon momentum squared, we can take for it the expectation value of  $-\vec{\nabla}^2$  for the kaonic wave functions. This leads to

$$\text{d) } b \vec{k}^2 \rightarrow b [(\omega - V_C)^2 - \mu^2 - \Pi] \quad (7)$$

Also since the potential is complex we can take the more symmetrical situation  $(b\vec{k}^2 + \vec{k}^2 b)/2$ , in which case we obtain the real part of the expression in Eq. (7)

$$e) b \vec{k}^2 \rightarrow b \operatorname{Re} [(\omega - V_C)^2 - \mu^2 - \Pi] \quad (8)$$

The energies and shifts for the energy dependent potential can be obtained by iteration. Given the smallness of the pieces under consideration the convergence is extremely fast.

## 4 Threshold behaviour and the low density limit

Eqs. (3) require the evaluation of the derivatives of the kaon selfenergy with respect to  $\vec{k}^2$  and  $k^0$  at threshold. However, these magnitudes are problematic when one goes to small densities, as we shall see. The problems stem from the behaviour of the free  $t$  matrix at threshold which has a cusp. This is related to the contribution of the elastic channel  $K^-N \rightarrow K^-N$  and hence, for the discussion, one can neglect all the other channels. Also the discussion here is completely general and thus we do not particularize to the  $K^-N \rightarrow K^-N$  reaction.

### 4.1 Behaviour of the elastic rescattering terms

To simplify the discussions we shall take unity for the transition potential  $K^-N \rightarrow K^-N$ . We begin with the study of the second order rescattering term with this potential, see Fig. 1. This is the term studied in the appendix of Ref. [30], which there led to coefficients  $b$  and  $c$  behaving like  $k_F^2$  in the limit of low densities, a result that would seem to violate the low density theorem.

In order to clarify the problems let us write the kaon selfenergy for this rescattering term

$$\Pi^{res}(k^0, \vec{k}, \rho) = 4 \int \frac{d^3 p}{(2\pi)^3} \int \frac{d^3 q}{(2\pi)^3} \frac{1}{2\omega(q)} \frac{n(\vec{p}, \rho)[1 - n(\vec{p} + \vec{k} - \vec{q}, \rho)]}{k^0 - \omega(q) + \varepsilon(\vec{p}) - \varepsilon(\vec{p} + \vec{k} - \vec{q}) + i\eta}, \quad (9)$$

where we use relativistic energies for the meson but non-relativistic ones for the nucleon, in order to be able to use explicit formulae for the Lindhard functions. In the following, we will denote the meson and nucleon masses by  $m$  and  $M$ , respectively. We have written explicitly the integral over the Fermi sea momentum,  $\vec{p}$ , and over the meson momentum,  $\vec{q}$ . Let us examine the behaviour of the  $\vec{q}$  integral in Eq. (9) in the limit of zero Fermi momentum and  $\vec{k} = 0$ . In such a case one gets

$$t^{res}(k^0, \vec{k} = 0) = \frac{4\pi}{(2\pi)^3} \int q^2 dq \frac{1}{2\omega(q)} \frac{1}{k^0 - \omega(q) - \frac{q^2}{2M} + i\eta}, \quad (10)$$

which would give us  $t^{res}$ , which is the contribution of the rescattering term to the free  $t$  matrix, as a function of  $k^0$ . Now let us find out the derivative of this function with respect

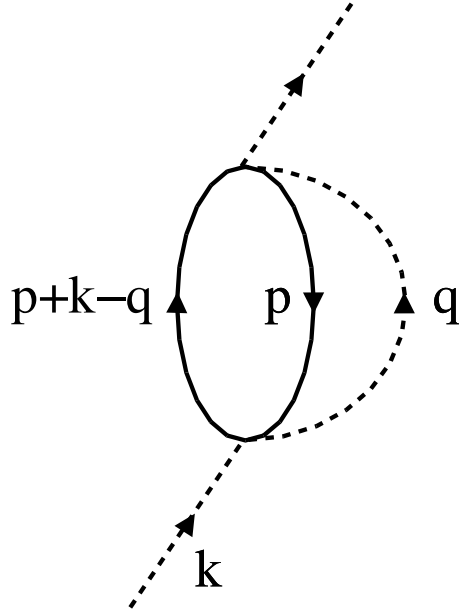


Figure 1: Second order rescattering contribution to the meson selfenergy.

to  $k^0$  and particularize for  $k^0 = m$ . Commuting the partial derivative and the integral, and concentrating in the region of small  $q$ , one finds an infrared divergence of the type

$$\int dq \frac{1}{q^2} \quad (11)$$

Certainly, as one puts a finite, even if small, Fermi momentum, the divergence disappears, and one finds a  $1/k_F$  behaviour, similarly to the derivative of the function  $I(\omega, 0)$  with respect to  $\omega$  in the appendix of [30]. Obviously, the divergence is recovered in the strict limit of  $k_F = 0$ . This is a subtle problem. One reason is that we have a branch point at threshold and the commutation of the derivative and the integral made above is not justified. Indeed, one can do the integration with respect to  $q$ , in Eq. (10), analytically and, after renormalization of the ultraviolet behaviour, the integral can be obtained from the two particle loop integral,  $J_0$ , given in appendix A of [32]. The difference is that in Eq. (10) we use a non-relativistic propagator for the nucleon, but since we are concerned about the infrared divergence it does not make any difference. Then one can study the derivative with respect to  $k^0$ . The expression for the loop function is:

$$t^{res}(k) \simeq 2M J_0(k^2) \equiv 2M i \int \frac{d^4q}{(2\pi)^4} \frac{1}{(q^2 - M^2 + i\eta)} \frac{1}{((q+k)^2 - m^2 + i\eta)},$$

where the approximation sign is present because the l.h.s. of the equation is the baryon

non-relativistic approach to the r.h.s. expression. Removing constant subtraction terms irrelevant for the discussion, this expression [32] is given by

$$(4\pi)^2 J_0(s) = \left(1 - \frac{(M-m)^2}{s}\right) \sigma \ln \frac{\sigma+1}{\sigma-1} + \frac{M^2-m^2}{s} \ln \frac{M}{m},$$

$$\sigma = \sqrt{\frac{1 - \frac{(M+m)^2}{s}}{1 - \frac{(M-m)^2}{s}}}, \quad (12)$$

where  $s$  is the Mandelstam variable. Close to threshold (in this case  $s = (M+m)^2$ ), and above it, we can expand  $J_0(s)$  as

$$J_0(s) = \frac{1}{(4\pi)^2} \left( \left(1 - \frac{(M-m)^2}{s}\right) (-i\pi\sigma + 2\sigma^2 + \mathcal{O}(\sigma^4)) + \frac{M^2-m^2}{s} \ln \frac{M}{m} \right), \quad (13)$$

and then we can perform the derivative with respect to  $s$  and find  $\left(\frac{\partial\sigma}{\partial s} = \frac{2mM}{\sigma(s-(M-m)^2)^2}\right)$  at threshold from above:

$$\frac{\partial J_0(s)}{\partial s} = \frac{1}{(4\pi)^2} \frac{1}{(M+m)^2} \left( -i\frac{\pi}{2\sigma} + 2 - \frac{M-m}{M+m} \ln \frac{M}{m} + \mathcal{O}(\sigma) \right). \quad (14)$$

Thus, what we find is that, since  $\sigma$  goes to zero at threshold, the derivative of the imaginary part goes to infinity but the derivative of the real part remains finite. This is related to the fact that the imaginary part goes as the momentum of the particle, and then its derivative with respect to  $s$  is infinite at threshold. Below threshold  $\sigma$  becomes purely imaginary and therefore  $\partial J_0(s)/\partial s$  is purely real and it diverges at threshold. This is logical since the analytical continuation below threshold of the imaginary part above threshold becomes real and this is the reason for the infinite derivative. Hence, the derivative of  $J_0(s)$  with respect to  $s$ , and therefore that with respect to  $k^0$  when  $\vec{k} = 0$ , takes different values at the right hand side than at the left hand side of the threshold point.

The results are then different from what one obtains by commuting the integral and the derivative, as we did before in Eq. (10) to obtain the divergence of Eq. (11). However, the fact remains that there are divergences. Nevertheless, this analytical study has served to see that the origin of the divergence is the existence of the imaginary part in the free  $t$ -matrix close and above threshold. This realization is important because, as we shall see, for finite values of  $\rho$ , the effect of Pauli blocking drastically reduces the imaginary part of the rescattering term of the meson selfenergy close to threshold, and what is more important it can be differentiated with respect to  $k^0$ . In order to see this, we perform first the integration over the Fermi sea in Eq. (9) and write the meson selfenergy as

$$\Pi^{res}(k^0, \vec{k} = 0, \rho) = \int \frac{d^3q}{(2\pi)^3} \frac{1}{2\omega(q)} U(k^0 - \omega(q), q, \rho), \quad (15)$$

where  $U$  is the Lindhard function for forward going particle-hole excitation. The ordinary Lindhard function contains also the backward going particle-hole term. For this reason



we give in the appendix the explicit expressions for the forward going contribution to the Lindhard function needed here. Inspection of Eq. (9) tells us that there is only imaginary part for  $k^0 - \omega(q) > 0$ .

It is easy to prove, using the formula for  $\text{Im } U$  of the appendix, that, for  $k^0 - m \ll k_F^2/2M$ ,  $\text{Im } \Pi^{res}(k^0, 0, \rho)$  goes as  $(k^0 - m)^2$ , but we save the proof here since this is a well known result for the imaginary part of the selfenergy of any particle in a medium [34–36]. This result is important because then the imaginary part of the meson selfenergy and its derivative with respect to  $k^0$  are continuous at threshold (actually for this rescattering contribution both the imaginary part of the function and its derivative vanish at threshold). Hence, the singularity in the derivative of the imaginary part of the free  $t$  matrix above threshold, which we have seen in Eq. (14), disappears in the meson selfenergy at finite densities. The use of dispersion relations in the selfenergy and its derivative then guarantee that both the real part of the selfenergy and its derivative are also continuous at threshold. Let us show this in a quantitative manner.

In Fig. 2 we show the real part of the meson selfenergy from this rescattering piece for  $k_F = 100$  MeV, corresponding to  $\rho = 0.05\rho_0$ , 50 MeV ( $\rho = 0.006\rho_0$ ) and 10 MeV ( $\rho = 0.00005\rho_0$ ) divided by  $\rho$  for normalization, and we compare the results with the real part of the free  $t$  matrix for the meson nucleon interaction from the corresponding rescattering term,  $t^{res}$ . We observe, indeed, that for finite densities the meson selfenergy is a regular function and shows no cusp, which is clearly visible in the free  $t^{res}$  matrix. It is interesting to see that for very small densities (see the curve corresponding to  $k_F = 10$  MeV in the figure)  $\Pi^{res}/\rho$  goes like the free  $t^{res}$  matrix, except for the fact that Pauli blocking has provided a regularization around the cusp. It is also interesting to observe that even at  $k_F = 50$  MeV, and certainly at  $k_F = 100$  MeV, one obtains practically a linear function in  $k^0$ . We can thus anticipate that problems linked to the original discontinuity of the derivative in the  $t$  matrix will have negligible effects in the evaluation of any observable where the different densities will have to be weighed in the nucleus. However, the formal problem still remains, because one has to define the derivatives at threshold for any density and, even if now they can be calculated, for very small densities (see e.g. the case of  $k_F = 10$  MeV) the function around threshold is by no means linear in  $k^0$ . Hence, if one takes a linear extrapolation based on the derivative at threshold, see Eq. (2), it is obvious from the figure that it would lead to a strong diversion from the actual calculated values of the selfenergy.

As we have mentioned, the problem is a formal one affecting only to small densities which should have no relevance in practical problems provided a sensible and realistic approach is taken. Yet, this might not be always easy to achieve. As an example we could consider a sensible approach the one in [30], where, according to the authors, they "artificially modify the slope of the function such that it is zero at  $k_F = 0$  but agrees to good accuracy with  $b_{eff}(k_F)$  for  $k_F > 50$  MeV ". However, the final effect of the nonlocalities on the calculated level shifts and widths in that work is substantially larger than we find here when treating carefully the nucleus as a finite system, as described below.

Indeed, the problems mentioned above do not appear in a finite nucleus. This issue was already addressed in [37] in a different problem, the study of the effect of core polarization

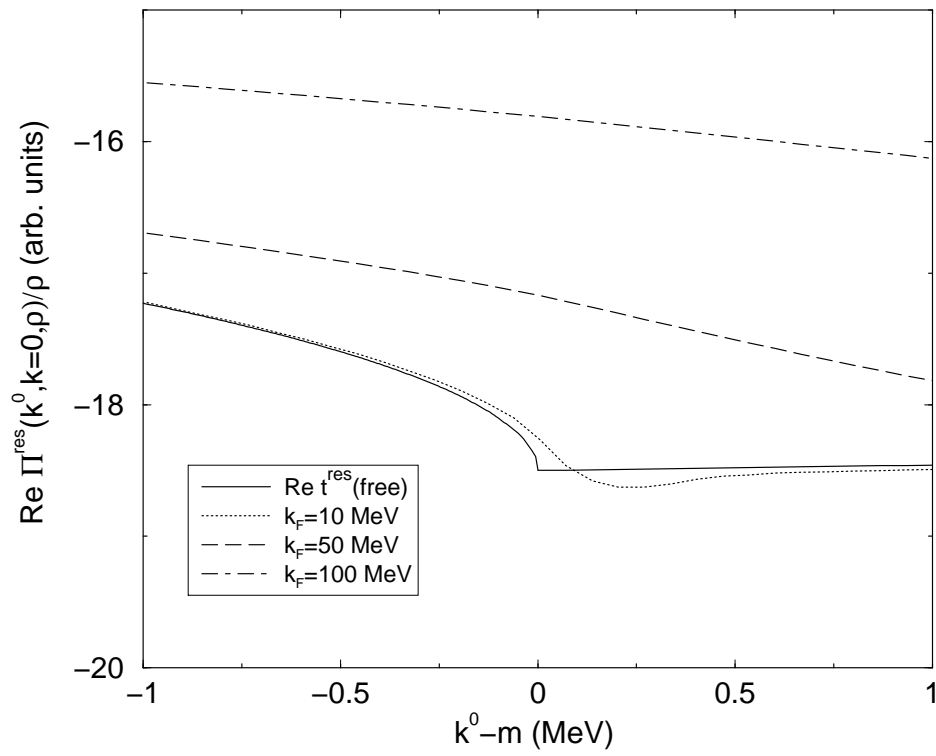


Figure 2: Real part of the kaon rescattering selfenergy,  $\Pi^{res}$ , of Eq. (9) divided by  $\rho$  as a function of  $k^0 - m$  for different densities.

on inelastic or charge exchange pion nucleus reactions. The reason is simple but subtle. If one looks at the expression of the Lindhard function, which results from removing the integral over  $d^3q/(2\pi)^3$ , the factor  $1/2\omega(q)$  and setting  $q = 0$  in Eq. (9), and one takes the threshold value  $k^0 = m$  and  $k = 0$ , one realizes that there is an indetermination of the type  $0/0$  in the integrand. The analytical expression of the Lindhard function is such that its limit for  $k \rightarrow 0$  is finite. Yet, in a closed shell nucleus the numerator of the equivalent response function is zero because it involves a matrix element  $\langle \phi_1 | \exp(i\vec{k}\vec{r}) | \phi_2 \rangle$ , where  $\phi_1$  would correspond to an occupied state and  $\phi_2$  to an excited state and these functions are orthogonal. However, the denominator would involve  $\epsilon_i - \epsilon_j$ , which is strictly non zero because there is a minimum excitation energy from the occupied states to the excited states. Thus, the corresponding response function in a finite nucleus is strictly zero while the Lindhard function does not vanish because of the continuity of the energies in the Fermi sea in infinite nuclear matter. Rather than doing an unnecessarily complicated evaluation in a finite nucleus, a simple solution to the problem was given in [37], including a finite excitation energy in the particle state, which we shall call the gap,  $\Delta$ , and reevaluating the Lindhard function, which then turned out to be strictly zero in the limit of small  $\vec{k}$ . The expressions for the Lindhard function with the gap can be found in the appendix of [37], however they include forward and backward propagating  $ph$  excitations. We need here only the forward propagating  $ph$  excitation according to Fig. 1, and since we perform evaluations with this new function in what follows, we give the explicit expression for this function in the appendix. Once the gap is included, the rescattering term of the meson selfenergy,  $\Pi^{res}$ , has imaginary part only for  $k^0 > m + \Delta$  and, thus, around  $k^0 = m$ , the relevant region for kaonic atoms, it is purely real. The gap is physical and it is about 1-3 MeV for most of the nuclei we analyze here. So, our strategy will be, first to show that once the gap is included the selfenergy can be accurately approximated by a linear function of  $k^0$  around  $k^0 = m$ . Second, to test that the results for kaonic atoms are rather insensitive to the gap value, with changes on the shifts and widths far smaller than the experimental uncertainties.

In Fig. 3 we show the results for the real part of the rescattering term of the meson selfenergy divided by  $\rho$  for different densities and compare them with the real part of the free  $t^{res}$  matrix including the gap in the particle energy, this is to say, we increase the nucleon mass in the intermediate state of the rescattering term by the gap energy, i.e, we add  $(-\Delta)$  in the denominator of Eq. (10). We have chosen here a gap of 3 MeV. The function around threshold is now well behaved for any density, showing a linear dependence in  $k^0$ , and we can see that for values of  $k_F$  around 50 MeV the meson selfenergy divided by  $\rho$  and the free  $t^{res}$  matrix differ in less than two percent and they are practically indistinguishable at  $k_F = 10$  MeV, a consequence of the low density theorem for the meson selfenergy [38–40].

We did not yet pay attention to the dependence of the selfenergy on  $\vec{k}^2$ , but the same arguments as above can be repeated. Again we can see in Fig. 4 that, once the gap energy is considered, the dependence is smooth around threshold,  $\vec{k}^2 = 0$ , and the selfenergy divided by  $\rho$  merges to the free  $t^{res}$  matrix as a necessary consequence of the low density theorem. Here  $t^{res}(k^0 = m, k)$  is defined as in Eq. (10) by changing  $\vec{q}^2/2M$  by  $(\vec{k} - \vec{q})^2/2M$

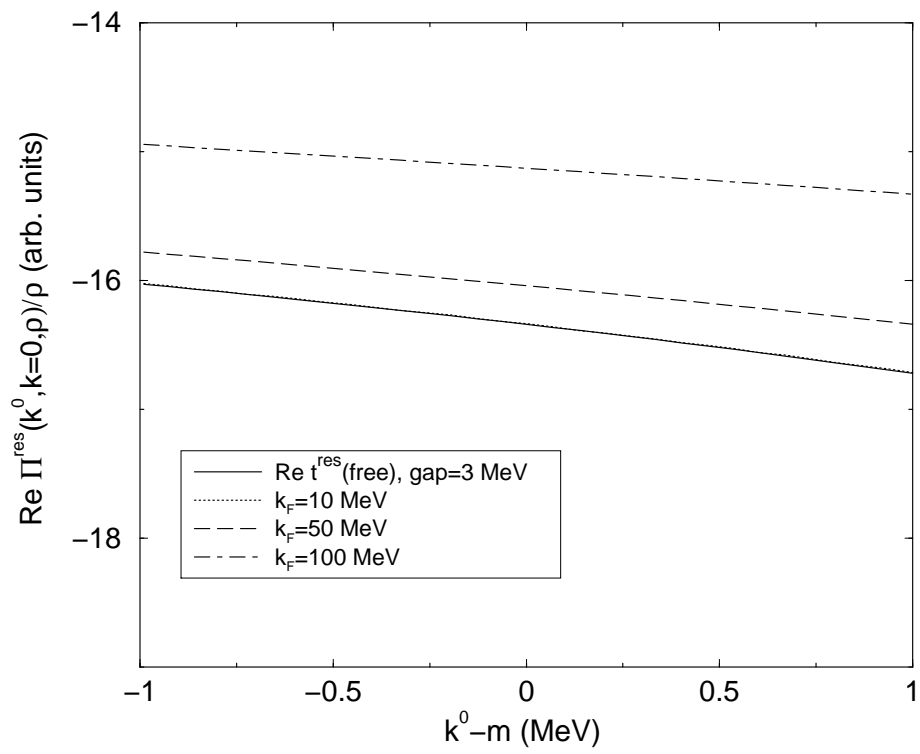


Figure 3: Same as Fig. 2, but including a gap of 3 MeV in the nucleon particle energy.

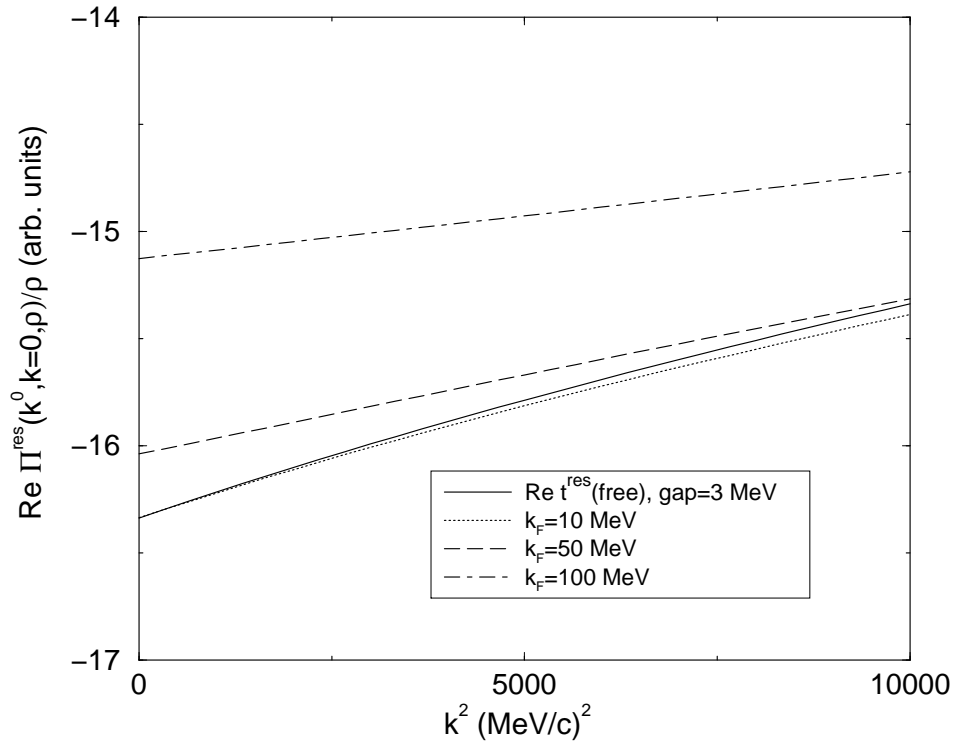


Figure 4: Real part of the rescattering term contribution to the meson selfenergy,  $\Pi^{\text{res}}$ , divided by  $\rho$  as a function of  $k^2$  for different densities, evaluated including a gap of 3 MeV in the nucleon particle energy.

(and adding  $(-\Delta)$  in the denominator).

The study conducted above has served to show the problems in the low density limit close to threshold due to the cusp behaviour of the free  $t$  matrix, but we have also seen that, once a physical value of the gap is introduced, all the problems disappear and one can also rely on the low density limit in order to evaluate values of the selfenergy and their derivatives with respect to  $k^0$  and  $\vec{k}^2$  at low densities.

## 4.2 Behaviour of the full kaon selfenergy

Now we come back to the realistic situation of the kaon selfenergy including all coupled channels in the calculation. We have learned from the previous section that the kaon selfenergy does not behave linearly in  $k^0$ ,  $\vec{k}^2$  around thresholds. We have avoided these problems around the  $K^-N$  threshold by means of the gap  $\Delta$ . The rest of the thresholds, like  $\pi\Sigma$ ,  $\eta\Lambda$ , etc., are far from the region of energy and momenta met by the  $K^-$  atoms, and hence these other coupled channels do not affect the linear behaviour of the kaon selfenergy for kaonic atoms. We will obtain the low density limit simply taking the selfenergy equal to  $t\rho$ , where  $t$  stands now for the average of  $t_{K^-N}$  over protons and neutrons evaluated including the gap energy for the intermediate nucleon state in the Bethe–Salpeter equation. Thus, in the limit of  $\rho$  going to zero we obtain

$$\begin{aligned} \left. \frac{\partial \Pi(k, \rho)}{\partial \vec{k}^2} \right|_{(\omega=m_K, \vec{k}=0)} &= - \left. \frac{\partial t}{\partial s} \right|_{(0)} \rho \\ \left. \frac{\partial \Pi(k, \rho)}{\partial \omega} \right|_{(\omega=m_K, \vec{k}=0)} &= \left. \frac{\partial t}{\partial s} \right|_{(0)} 2(m_K + M_N)\rho, \end{aligned} \quad (16)$$

where the label (0) indicates that the derivative is taken at threshold. This means that the values of  $b(\rho)$  and  $c(\rho)$  from Eqs. (3) can be cast in the low density limit as

$$\begin{aligned} \left. \frac{b(\rho)}{\rho} \right|_{\rho=0} &= - \left. \frac{\partial t}{\partial s} \right|_{(0)} \\ \left. \frac{c(\rho)}{\rho} \right|_{\rho=0} &= \left. \frac{\partial t}{\partial s} \right|_{(0)} 2(m_K + M_N), \end{aligned} \quad (17)$$

and the above relationships are the constraints we impose to the low density behaviour of the parameters  $b(\rho)$  and  $c(\rho)$ . Note that these coefficients are now complex because of the inclusion of the non-elastic channels.

In Figs. 5 and 6 we can see the numerical results obtained for the partial derivatives of the kaon selfenergy as a function of the density. In order to stress the low density behavior we have also shown them divided by the density plotted against the Fermi momentum. The density and Fermi momentum are in units of  $\rho_0 = 0.17 \text{ fm}^{-3}$  and  $k_{F0} = 268.4 \text{ MeV}$ , respectively. We also show the results calculated with the two values of the gap energy, 1 MeV and 3 MeV.

As one can see in the figures, the values of the partial derivatives have a density dependence that makes the derivatives positive and negative. Thus, there are subtle cancellations

when evaluating the results with the potential of Eq. (2) because, even if the derivatives act on the potential which depends on the nuclear density, the physical meaning is that one should be producing the kaon momentum which is a small quantity. Hence, the necessary cancellations have to appear in the integrals involving the derivatives of the density, which measure nucleon momenta, to finally account for the small kaon momenta. This is the reason why so much emphasis has to be made on the low density limit because, as one can see in Fig. 5, the low density limit for the partial derivative with respect to  $\vec{k}^2$  forces a change of sign of the derivatives with respect to  $\rho$  which will appear when the  $\vec{\nabla}$  operator acts on the  $\rho$  dependent functions of the potential.

## 5 P-waves

The lowest order meson-baryon Lagrangian [42] can be written as

$$L_1^{(B)} = \langle \bar{B}i\gamma^\mu\nabla_\mu B \rangle - M_B\langle \bar{B}B \rangle + \frac{1}{2}D\langle \bar{B}\gamma^\mu\gamma_5\{u_\mu, B\} \rangle + \frac{1}{2}F\langle \bar{B}\gamma^\mu\gamma_5[u_\mu, B] \rangle, \quad (18)$$

where the symbol  $\langle \rangle$  stands for the trace of the SU(3) matrices B, involving the baryon fields of the octet of the nucleon, and  $u_\mu$ , involving the meson fields of the octet of the pion. The constants  $D$  and  $F$  are given by  $D + F = g_A = 1.257$  and  $D - F = 0.33$ . The term involving the covariant derivative gives rise to a contact s-wave term, which is evaluated in [24], and a contact p-wave term which we write here in Eq. (19) in the center of mass (CM) frame of the  $\bar{K}N$  state

$$t^{(p,C)} = -C_{ij}\frac{1}{4f^2}\left(\frac{E_i + M_i}{2M_i}\right)^{1/2}\left(\frac{E_j + M_j}{2M_j}\right)^{1/2}\left(\frac{1}{2M_i} + \frac{1}{2M_j}\right)\vec{\sigma}\vec{k}'\vec{\sigma}\vec{k}, \quad (19)$$

with  $M_{i,j}$ ,  $E_{i,j}$ , the mass and energy of the initial and final baryons, and  $C_{ij}$  SU(3) coefficients which are tabulated in [24]. The variables  $\vec{k}'$  and  $\vec{k}$  are the center of mass momenta of the outgoing and incoming meson, respectively.

In addition we also have the contribution of the  $\Lambda$ ,  $\Sigma$  and  $\Sigma^*$  pole diagrams with two vertices of the type  $KNY$ , with  $Y$  being the hyperon, which come from the  $D$  and  $F$  terms of Eq. (18) and that can be easily evaluated [43, 44].

Unlike the  $\Lambda(1405)$  resonance, which is generated dynamically from the lowest order s-wave chiral Lagrangians and multiple scattering, the strength of the p-wave interaction is too small to generate dynamically the  $\Sigma^*(1385)$ , which, in the language of refs. [45, 46], would then qualify as a genuine, or preexisting, resonance built up mostly from three-quark states. Thus, we follow a phenomenological approach to include the contribution from  $\Sigma^*h$  excitations. The  $KN\Sigma^*$  vertex is evaluated in [44] by means of SU(6) symmetry, in analogy to the evaluation of the  $\pi\Delta N$  vertex from the  $\pi NN$  one. It differs slightly from the one used in [43], where SU(3) arguments are used.

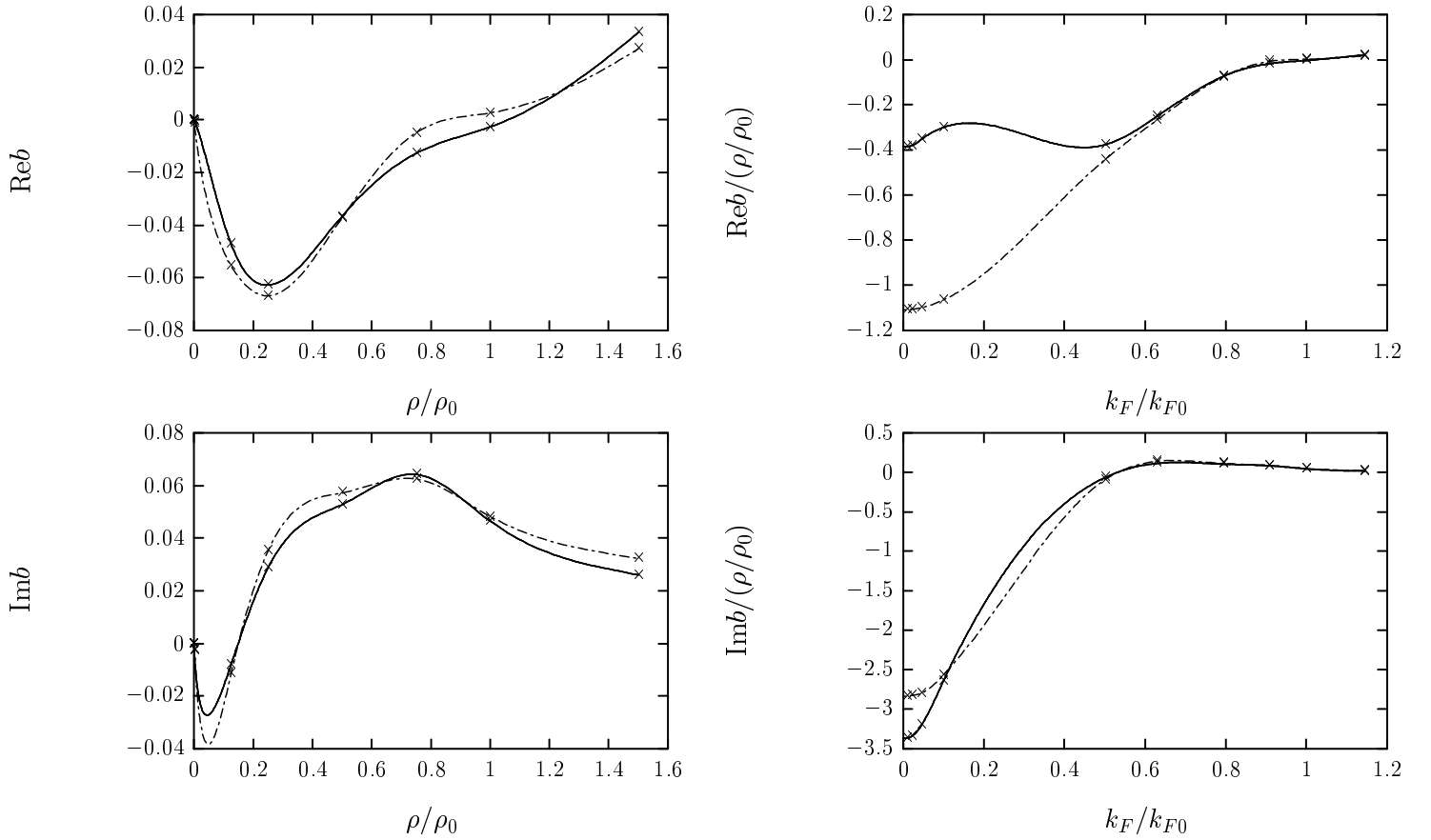


Figure 5: The real and imaginary parts of  $b$  versus  $\rho/\rho_0$  are depicted in the two left figures. The real and imaginary parts of  $[b/(\rho/\rho_0)]$  versus  $k_F/k_{F0} \equiv (\rho/\rho_0)^{1/3}$  are shown on the right panels. The crosses correspond to the points which have been numerically evaluated from Eqs. (1), (3) and (17) and the lines are the interpolated values, which have been used for calculations. The solid lines have been obtained using an energy gap of  $\Delta = 1$  MeV and the dashed ones with  $\Delta = 3$  MeV.



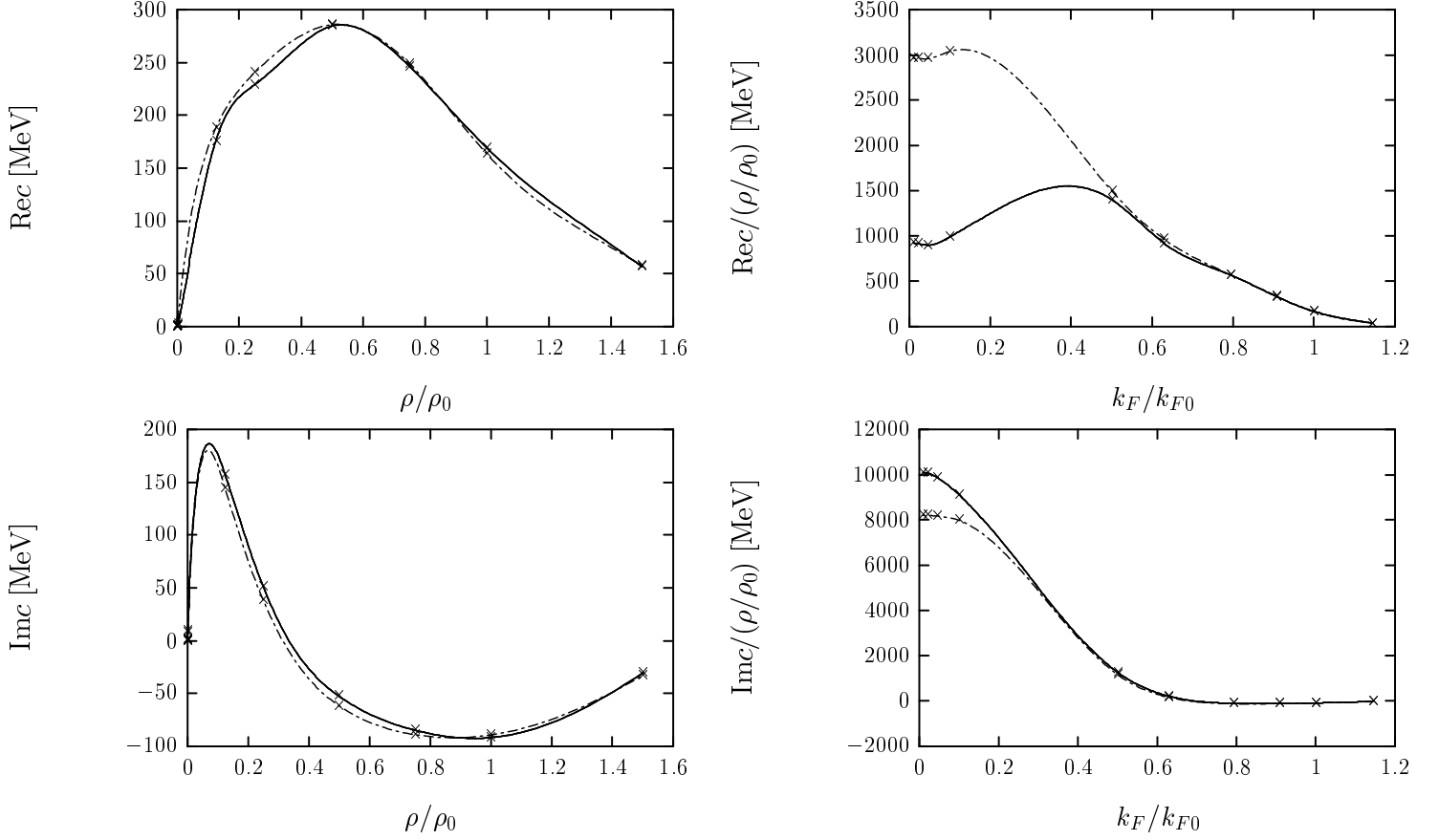


Figure 6: The left figures show the real and imaginary parts of  $c$  versus  $\rho/\rho_0$ . The real and imaginary parts of  $[c/(\rho/\rho_0)]$  versus  $k_F/k_{F0} \equiv (\rho/\rho_0)^{1/3}$  are shown in the figures on the right-hand side. The crosses correspond to the points which have been numerically evaluated from Eqs. (1) , (3) and (17) and the lines are the interpolated values for arbitrary density.  $c$  has been obtained from  $\Pi$  calculated without pion selfenergy for  $\rho/\rho_0 \leq 0.25$ . The solid lines have been obtained using an energy gap of  $\Delta = 1$  MeV and the dashed ones with  $\Delta = 3$  MeV.

For the case of  $\Lambda$  and  $\Sigma$  pole terms the expressions that we get for the p-wave amplitude in the CM are

$$t^{(p,Y)} = D_{M'B'Y} D_{MBY} \left(1 + \frac{k'^0}{2M_{B'}}\right) \left(1 + \frac{k^0}{2M_B}\right) \frac{1}{\sqrt{s} - M_Y} \vec{\sigma}_{k'} \vec{\sigma}_k ; Y = \Lambda, \Sigma \quad (20)$$

where the subindices  $M, B$  ( $M', B'$ ) stand for the initial (final) meson, baryon. The quantities  $D_{MBY}$  are SU(3) coefficients given by

$$D_{MBY} = c_{DY} \sqrt{\frac{20}{3}} \frac{D}{2f} - c_{FY} \sqrt{12} \frac{F}{2f} \quad (21)$$

where the  $c_{DY}, c_{FY}$  coefficients are given in table 1, and  $f = 1.15 f_\pi$  as in ref. [24].

Similarly, in the case of the  $\Sigma^*$  pole term the amplitude in the CM is given by

$$t^{(p,\Sigma^*)} = D_{M'B'\Sigma^*} D_{MB\Sigma^*} \frac{1}{\sqrt{s} - M_{\Sigma^*}} \vec{S}_{k'} \vec{S}_k^\dagger, \quad (22)$$

where the  $D$  coefficient is given by

$$D_{MB\Sigma^*} = c_S \frac{12D + F}{5} \frac{1}{2f} \quad (23)$$

and  $c_S$  is tabulated in table 1.

Table 1: Coefficients for the  $K^- NY (K^- N\Sigma^*)$  couplings

	$c_{D\Lambda}$	$c_{F\Lambda}$	$c_{D\Sigma}$	$c_{F\Sigma}$	$c_S$
$K^- p$	$-\sqrt{\frac{1}{20}}$	$\sqrt{\frac{1}{4}}$	$\sqrt{\frac{3}{20}}$	$\sqrt{\frac{1}{12}}$	$-\sqrt{\frac{1}{12}}$
$K^- n$	0	0	$\sqrt{\frac{3}{10}}$	$\sqrt{\frac{1}{6}}$	$-\sqrt{\frac{1}{6}}$

In order to evaluate the p-wave selfenergy we write the amplitudes in terms of the kaon and nucleon variables in the frame where the nuclear Fermi sea is at rest. The former  $(1 + k^0/2M_B)\vec{\sigma}_k$  vertex of Eq. (20), which was given in the CM, becomes now

$$\vec{\sigma}_k \left(1 - \frac{k^0}{2M_Y}\right) - \frac{\vec{\sigma}_p}{2} k^0 \left(\frac{1}{M_N} + \frac{1}{M_Y}\right), \quad (24)$$

where  $\vec{p}$  is the nucleon momentum, and the combination of the two vertices gives

$$\vec{\sigma}_k \vec{\sigma}_k \left(1 - \frac{k^0}{2M_Y}\right)^2 + \frac{\vec{\sigma}_p \vec{\sigma}_p}{4} (k^0)^2 \left(\frac{1}{M_N} + \frac{1}{M_Y}\right)^2 \quad (25)$$

where we have already specified the forward direction of the kaons where the evaluation of the selfenergy in infinite matter is done.

On the other hand, for the  $\Sigma^*$  pole term we have to write the kaon momentum in the CM frame and then we have

$$\vec{k}_{CM} \simeq \vec{k} \left( 1 - \frac{k^0}{M_{\Sigma^*}} \right) - \frac{k^0}{M_{\Sigma^*}} \vec{p}. \quad (26)$$

Thus, the  $\vec{k}_{CM} \vec{k}_{CM}$  combination becomes

$$\vec{k}_{CM} \cdot \vec{k}_{CM} \simeq \vec{k} \vec{k} \left( 1 - \frac{k^0}{M_{\Sigma^*}} \right)^2 + \left( \frac{k^0}{M_{\Sigma^*}} \right)^2 \vec{p}^2. \quad (27)$$

The evaluation of the selfenergy corresponding to the diagrams of Fig. 7 can be written for symmetrical nuclear matter in terms of the Lindhard functions used in [44] as a p-wave part

$$\begin{aligned} \Pi_{K^-}^{(p)}(k^0, \vec{k}, \rho) &= \frac{1}{2} D_{K^-p\Lambda}^2 f_{\Lambda}^2 \vec{k}^2 U_{\Lambda}(k^0, \vec{k}, \rho) \\ &+ \frac{3}{2} D_{K^-p\Sigma^0}^2 f_{\Sigma}^2 \vec{k}^2 U_{\Sigma}(k^0, \vec{k}, \rho) \\ &+ D_{K^-p\Sigma^{*0}}^2 f_{\Sigma^*}^2 \vec{k}^2 U_{\Sigma^*}(k^0, \vec{k}, \rho) \\ &- \frac{3}{2} \frac{1}{4f^2} \frac{1}{M_N} f_c^2 \vec{k}^2 \rho \end{aligned} \quad (28)$$

where the recoil factors  $f_i$  are given by

$$\begin{aligned} f_{\Lambda} &= \left( 1 - \frac{k^0}{2M_{\Lambda}} \right) ; \quad f_{\Sigma} = \left( 1 - \frac{k^0}{2M_{\Sigma}} \right) \\ f_{\Sigma^*} &= \left( 1 - \frac{k^0}{M_{\Sigma^*}} \right) ; \quad f_c = \left( 1 - \frac{k^0}{M_N + k^0} \right) \end{aligned} \quad (29)$$

together with an induced piece of s-wave nature coming from the Fermi motion of the nucleons and the frame transformation ( $\vec{p}^2$  terms in Eqs. (25),(27)) which is given by

$$\Pi_{K^-}^{(s,ind)}(k^0, \vec{k}, \rho) = \frac{3}{5} k_F^2 (k^0)^2 (A_p \rho_p + A_n \rho_n) \quad (30)$$

where  $A_N (N = p, n)$  is given by

$$\begin{aligned} A_N &= \frac{1}{4} \left( \frac{1}{M_N} + \frac{1}{M_{\Lambda}} \right)^2 \frac{D_{K^-N\Lambda}^2}{\sqrt{s} - M_{\Lambda}} \\ &+ \frac{1}{4} \left( \frac{1}{M_N} + \frac{1}{M_{\Sigma}} \right)^2 \frac{D_{K^-N\Sigma}^2}{\sqrt{s} - M_{\Sigma}} \\ &+ \left( \frac{1}{M_{\Sigma^*}} \right)^2 \frac{D_{K^-N\Sigma^*}^2}{\sqrt{s} - M_{\Sigma^*}} \\ &- C_{K^-N, K^-N} \frac{1}{4f^2} \frac{1}{M_N} \left( \frac{1}{M_N + k^0} \right)^2 \end{aligned} \quad (31)$$

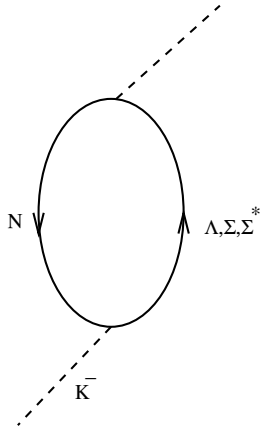


Figure 7: Diagram contributing to p-wave  $K^-$ -selfenergy via  $K^-N \rightarrow \Lambda$ ,  $K^-N \rightarrow \Sigma$  and  $K^-N \rightarrow \Sigma^*$  processes.

and  $C_{K^-p, K^-p} = 2$ ,  $C_{K^-n, K^-n} = 1$ . For the kaonic atom case the Lindhard function  $U_Y$  is given by:

$$U_Y(m_K, 0, \rho) = \frac{\rho}{m_K + M_N - M_Y + i\frac{1}{2}\Gamma_Y(\sqrt{s} = M_N + m_K)}, \quad Y = \Lambda, \Sigma, \Sigma^* \quad (32)$$

Since the momentum in the  $\vec{k}^2$  factor of Eq. (28) comes from the p-wave amplitudes and is already in the lab frame, the appropriate combination in finite nuclei, according to the findings of [27, 28], is  $\vec{k}^2 U_Y \rightarrow -\vec{\nabla} U_Y \vec{\nabla}$  and  $\vec{k}^2 \rho \rightarrow -\vec{\nabla} \rho \vec{\nabla}$ . The familiar ATT term (angular transform term) is here incorporated by means of the recoil factors  $f_i$  given in Eq. (29).

With all these ingredients we solve the KGE, Eq. (6), and show the results in the next section.

## 6 Numerical results

We solve the KGE of Eq. (6) with the microscopic antikaon-nucleus optical potential of ref. [13] (neglecting any isovector effects) plus the several non-local and p-wave terms discussed in the previous sections. As we already mentioned, for  $V_C(r)$  we use the Coulomb interaction taking exactly the finite-size distribution of the nucleus and adding to it the vacuum-polarization corrections [47].

The numerical solution of the Klein-Gordon equation is done using the method in coordinate space of [48]. The densities used throughout this work are those compiled in ref. [9]. However charge (neutron matter) densities do not correspond to proton (neutron) ones because of the finite size of the proton (neutron). We take that into account following the lines of ref. [28].

In the present work we have used a  $K^-$  selfenergy calculated in symmetric nuclear matter. For heavy nuclei having a neutron excess our results could be easily improved by weighting the proton and neutron contributions to the selfenergy in Eq. (1) with the factors  $Z/(A/2)$  and  $N/(A/2)$ , respectively. However, for the purpose of the present work, which is to establish the role of p-wave pieces and non-localities associated to s-wave, we have not considered necessary to implement these changes.

## 6.1 P-Wave and non-local effects.

We solve the KGE using different options to account for the non-local terms of the  $K^-$  selfenergy, II. For each one of these options, the KGE has been solved for a set of 63 shifts and widths of kaonic atoms levels<sup>1</sup>. Shifts and widths for all models are given in table 2 (gap  $\Delta = 1$  MeV) and table 3 (gap  $\Delta = 3$  MeV) for a set of selected typical levels of kaonic atoms across the periodic table. To better quantify the changes we also give  $\chi^2$  per number of data. As can be appreciated in tables the effects on the spectra of both the p-wave pieces, discussed in section 5, and the non-local terms, coming from the dominant s-wave potential of ref. [13] when the zero range approximation is relaxed, are small when compared to the experimental uncertainties. By comparing  $\chi^2/N = 3.76$  for row (1), where only the s-wave local optical potential is considered, with the values of  $\chi^2/N$  for rows (2), (3a), (3b), (3c), (3d), (3e) and (4), where different nonlocal and p-wave effects are added, we see that  $\chi^2/N$  change at most by  $\pm 0.7$ . Then we conclude that the effects of these nonlocal contributions on the kaonic atoms spectra are smaller than the experimental errors. Comparison of the results in the two tables shows that they are also rather independent of the value of the gap. Thus, despite some theoretical ambiguities in the nonlocal terms, for practical purposes they can be safely ignored.

The small effect of the p-waves on the shifts and widths found here was also noted in ref. [3], where the p-wave piece coming from  $\Sigma^*h$  excitations was included. Their p-wave contribution to the antikaon selfenergy turned out to be very small compared to the s-wave one (see Fig. 7 in ref. [3]) and made only a “minor contribution” to the atomic shifts and widths.

## 6.2 $\Sigma^*$ -hole excitation effects on the selfconsistent determination of the s-wave $K^-$ -selfenergy.

In this subsection we report on the role played by the  $\Sigma^*h$ -excitation when it is included in the self-consistent calculation of the s-wave  $K^-$  potential. In ref. [13], only the  $\Lambda h$ - and  $\Sigma h$ -p-wave terms were included in the selfconsistent calculation of the dominant s-wave antikaon-nucleus potential. The results obtained with this potential were reported in refs. [8] and [9], and have served us here, see row (1) in tables 2 and 3, as a reference to evaluate the effect of the non-local and p-wave terms studied in this paper. In a latter work, ref. [44], in addition to the  $\Lambda h$ - and  $\Sigma h$ - p-wave terms, the  $\Sigma^*$ -hole excitation term

---

<sup>1</sup>This set of data is the same used in [9]

of Fig. 7 was included in the selfconsistent evaluation of  $s$ -wave  $K^-$ -selfenergy, as well. With this new potential, a better description of the kaonic atom data is achieved. Indeed, this improved  $s$ -wave potential provides<sup>2</sup> a  $\chi^2/N = 2.89$  to be compared to the value of 3.76 provided by the original potential of ref. [13]. In Fig. 8 we show the  $s$ -wave  $K^-$ -optical potential both, with and without  $\Sigma^*h$ -excitation in the selfconsistent evaluation. Differences between both potentials are moderately small for the low densities relevant in kaonic atoms, but have a significant density dependence. At low densities, the inclusion of the  $\Sigma^*h$ -term leads to smaller, in absolute value, values for both the imaginary and real parts of the potential. Thus, there are two competing effects: reduction of the attraction because of a smaller real part and a reduction of the repulsion (increase of the attraction) because of a smaller imaginary part. It seems, that the latter effect is bigger than the former one and the resulting effect is an increase of the attraction which leads to a better description of the data in agreement with the findings of ref. [9]. Thus, the new potential provides bigger widths and smaller, in absolute value, shifts than the one of ref. [13].

In the row labeled  $(1)_{\Sigma^*}$  of table 2, we present the results for selected kaonic atom levels which are obtained by using only the  $s$ -wave optical potential which includes the  $\Sigma^* - h$  excitation in the selfconsistent evaluation of the  $s$ -wave  $K^-$  selfenergy, with a vanishing value of the gap. By comparing this row with row (1) of the same table, we see that the inclusion of the  $\Sigma^* - h$  excitation in the selfconsistent evaluation of the  $s$ -wave  $K^-$  selfenergy improves the global agreement between the theoretically predicted values and the the empirical ones. We should note that unlike the nonlocal effects which depend on the prescription, the inclusion of the  $\Sigma^* - h$  correction in the  $s$ -wave  $K^-$  selfenergy, although it has a moderate effect, is well defined. On the other hand, considering again only the  $s$ -wave  $K^-$  selfenergy, the effect of including non vanishing gap values of about  $\Delta = 1 \sim 3$  MeV has a very small effect on the shifts and widths of the known kaonic levels. This small effect can be quantified by observing that, for the considered set of data, the values  $\chi^2/N = 2.89$  for  $\Delta = 0$ ,  $\chi^2/N = 2.83$  for  $\Delta = 1$  MeV and  $\chi^2/N = 2.94$  for  $\Delta = 3$  MeV, which we obtain using only the  $s$ -wave  $K^-$  selfenergy, are very close.

## 7 Conclusion

We have concentrated on the evaluation of corrections to the  $K^-$  nucleus optical potential originating from the momentum and energy dependence of the  $s$ -wave selfenergy, previously developed, plus corrections to this potential originating from the  $p$ -wave part of the elementary  $K^-N$  amplitudes. Some of the corrections lead to nonlocal terms in finite nuclei, and the fact that the calculations of the selfenergy are done previously using local approximations, like the assumption of a local Fermi sea, introduces some ambiguities in the choice of the form of the nonlocal potential. The use of several alternatives serves us to quantify the amount of intrinsic uncertainty in our approach.

---

<sup>2</sup>This value is obtained with a zero gap energy, and only very small changes are found for non-vanishing values of the gap energy.

	$\chi^2/N$	$^{10}_5\text{B}$		$^{27}_{13}\text{Al}$		$^{63}_{29}\text{Cu}$		$^{112}_{48}\text{Cd}$		$^{238}_{92}\text{U}$	
		$-\epsilon_{2p}$	$\Gamma_{2p}$	$-\epsilon_{3d}$	$\Gamma_{3d}$	$-\epsilon_{4f}$	$\Gamma_{4f}$	$-\epsilon_{5g}$	$\Gamma_{5g}$	$-\epsilon_{7i}$	$\Gamma_{7i}$
(1)	3.76	217	551	109	368	384	1121	528	1437	330	1090
(2)	4.00	213	542	110	362	392	1110	543	1420	350	1076
(3a)	3.20	211	565	102	397	361	1229	494	1588	302	1291
(3b)	4.00	234	564	118	383	415	1172	568	1515	357	1196
(3c)	4.01	234	564	118	383	415	1173	569	1515	358	1197
(3d)	4.02	233	562	118	382	414	1170	568	1511	356	1194
(3e)	3.38	219	568	110	383	391	1182	538	1528	336	1203
(4)	3.69	217	552	110	371	388	1141	534	1465	337	1166
(1) $_{\Sigma^*}$	2.89	208	575	105	398	373	1219	512	1550	320	1201
Exp	-	208	810	80	443	370	1370	400	2010	260	1500
		$\pm 35$	$\pm 100$	$\pm 13$	$\pm 22$	$\pm 47$	$\pm 170$	$\pm 100$	$\pm 440$	$\pm 400$	$\pm 750$

Table 2: Widths and shifts of representative kaonic atom levels in eV obtained from different potentials, taking always the energy gap equal to  $\Delta = 1$  MeV. Different cases correspond to the local potential of ref. [13] (for a comparison in row (1) we give the results obtained with  $\Pi(m_K, 0, \rho)$ , first term on the r.h.s. of Eq. (2)) . Rows (2) to (4) correspond to different additions to this dominant piece:

(2) Only p-wave Lindhard function non-local effects from Eq. (28) and the local induced term of Eq. (30) are added.

(3) Only  $b\vec{q}^2$  non-local effects, see Eq. (2), are included using different ways: (3a)  $-\vec{\nabla}b\vec{\nabla}$ , (3b)  $-\vec{\nabla}b\vec{\nabla} - 0.5(\Delta b)$ , (3c)  $-b\vec{\nabla}^2$ , (3d)  $b[(\omega - V_C)^2 - \mu^2 - \Pi]$ , (3e)  $b\text{Re}[(\omega - V_C)^2 - \mu^2 - \Pi]$ .

(4) Only  $c(\omega - \mu)$  “non-local” effects are added, see Eq. (2).

The results of row (1) $_{\Sigma^*}$  are obtained from a purely  $s$ -wave optical potential, like in row (1), but including  $\Sigma^* - h$  excitations as described in subsection 6.2. For each potential,  $\chi^2$  per number of data  $N$  is shown. We use a set of 63 shifts and widths previously used in ref. [9].

	$\chi^2/N$	$^{10}_5\text{B}$		$^{27}_{13}\text{Al}$		$^{63}_{29}\text{Cu}$		$^{112}_{48}\text{Cd}$		$^{238}_{92}\text{U}$	
		$-\epsilon_{2p}$	$\Gamma_{2p}$	$-\epsilon_{3d}$	$\Gamma_{3d}$	$-\epsilon_{4f}$	$\Gamma_{4f}$	$-\epsilon_{5g}$	$\Gamma_{5g}$	$-\epsilon_{7i}$	$\Gamma_{7i}$
(1)	3.76	217	551	109	368	384	1121	528	1437	330	1090
(2)	4.00	213	542	110	362	392	1110	543	1420	350	1076
(3a)	3.03	207	567	97	402	343	1254	469	1623	272	1335
(3b)	3.96	235	566	119	386	416	1187	569	1539	353	1225
(3c)	3.95	235	567	119	386	416	1188	569	1540	353	1225
(3d)	3.95	235	565	119	386	415	1184	567	1534	351	1220
(3e)	3.25	218	570	109	386	387	1193	531	1548	325	1227
(4)	3.65	217	552	109	371	386	1142	531	1479	330	1169
Exp	-	208	810	80	443	370	1370	400	2010	260	1500
		$\pm 35$	$\pm 100$	$\pm 13$	$\pm 22$	$\pm 47$	$\pm 170$	$\pm 100$	$\pm 440$	$\pm 400$	$\pm 750$

Table 3: Same as in table 2 but for an energy gap of  $\Delta = 3$  MeV

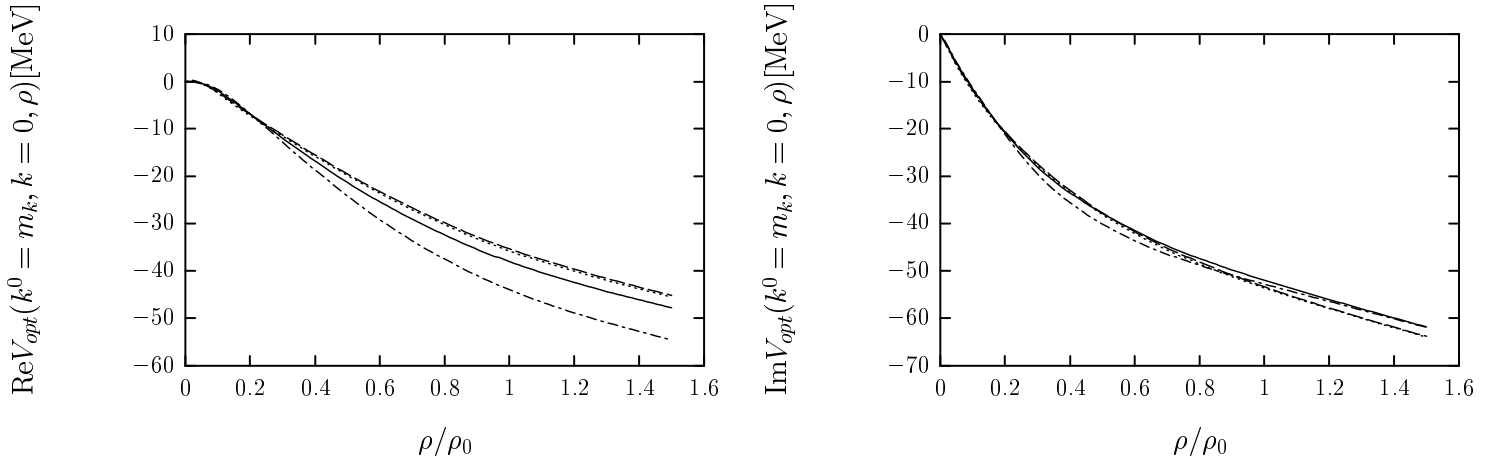


Figure 8: The real and imaginary parts of the  $K^-$  optical potential,  $V_{opt} = \Pi/(2m_K)$ , at energy  $k^0 = m_{K^-}$  and momentum  $k = 0$  versus  $\rho/\rho_0$ , are depicted in the figures. The selfenergy  $\Pi$  is evaluated from Eq. (1).

The solid lines have been obtained using no energy gap ( $\Delta = 0$ ), the dashed ones with  $\Delta = 1$  MeV and the dotted ones with  $\Delta = 3$  MeV. The dot-dashed lines correspond to the  $\Delta = 0$  and omitting the  $\Sigma^*$ -hole propagation of the  $K^-$  in the Bethe-Salpeter equations.



Fortunately, the corrections turn out to be small, smaller than the experimental errors, which gives support to the results obtained with only an s-wave optical potential, which has been the rule in the studies of kaonic atoms. We also make some choices of equivalent, energy dependent, potentials and find also small corrections. We have calculated widths and shifts for a large set of kaonic atoms. Although fits of better quality than the present results can be obtained, the potential has the merit of being a free parameter theoretical one which gives a fair reproduction of the data.

We have made a thorough study of the optical potential around threshold and have shown the mathematical problems that one faces at very low densities. They are related to the cusp in the elementary  $K^-N \rightarrow K^-N$  scattering amplitude at threshold, where some of the derivatives become infinite. The peculiar low density behaviour found in [30] is tied to these problems and a natural physical solution for them is found here by considering the finite excitation energy of real nuclei.

As with respect to the use of empirical potentials to analyze the kaonic atom data, our results endorse the approaches which are based exclusively on an s-wave optical potential, once we see that all nonlocal terms generated lead to corrections which are smaller than present experimental errors.

Another relevant finding of this paper is, that using a purely theoretical optical potential, a quite satisfactory description of the kaonic atom data is achieved. For 63 data, we find  $\chi^2/N = 2.89$ , using the s-wave local theoretical potential of ref. [44] which contains  $\Sigma^* - h$  excitations in the selfconsistent calculation of the s-wave  $K$  selfenergy.

## 8 Acknowledgment

We would like to thank A. Gal for discussions. This work is partly supported by DGICYT contracts PB96-0753, PB98-1247 and PB98-1367. We would also like to acknowledge support from the EU TMR Network Eurodaphne, contract no. ERBFMRX-CT98-0169, and from the Generalitat de Catalunya and Junta de Andalucía under grants 2000SGR-24 and FQM 0225 respectively.

## Appendix: the Lindhard function with a gap in the particle-hole excitation energy

We define the Lindhard function for the forward going particle-hole excitation as

$$U(q^0, q, \Delta, \rho) = 4 \int \frac{d^4k}{(2\pi)^3} \frac{n(\vec{k}, \rho)[1 - n(\vec{k} + \vec{q}, \rho)]}{q^0 + \varepsilon(\vec{k}) - \varepsilon(\vec{k} + \vec{q}) - \Delta + i\eta} . \quad (\text{A.1})$$

where the energy gap  $\Delta$  separates the occupied and unoccupied nucleon states. Through the paper in some situations we have referenced to  $U(q^0, q, \rho)$  which is obtained from

Eq. (A.1) above, setting the gap to zero. We find for  $x \leq 2$ :

$$\begin{aligned} \text{Re } U(q^0, q, \Delta, \rho) = & -\frac{2Mk_F}{\pi^2} \frac{1}{2x} \left\{ \frac{x}{2} - \frac{\nu - \delta}{4} + \frac{\nu - \delta}{2} \ln \left| \frac{\nu - \delta + x^2 - 2x}{\nu - \delta} \right| \right. \\ & \left. + \frac{1}{2} \left[ 1 - \frac{1}{4} \left( \frac{\nu - \delta}{x} - x \right)^2 \right] \ln \left| \frac{\nu - \delta - x^2 - 2x}{\nu - \delta + x^2 - 2x} \right| \right\}, \end{aligned} \quad (\text{A.2})$$

and for  $x \geq 2$ :

$$\text{Re } U(q^0, q, \Delta, \rho) = -\frac{2Mk_F}{\pi^2} \frac{1}{2x} \left\{ \frac{x}{2} - \frac{\nu - \delta}{2x} + \frac{1}{2} \left[ 1 - \frac{1}{4} \left( \frac{\nu - \delta}{x} - x \right)^2 \right] \ln \left| \frac{\nu - \delta - x^2 - 2x}{\nu - \delta - x^2 + 2x} \right| \right\}, \quad (\text{A.3})$$

where

$$\nu = \frac{2Mq^0}{k_F^2}, \quad x = \frac{q}{k_F}, \quad \delta = \frac{2M\Delta}{k_F^2}, \quad \rho = \frac{2k_F^3}{3\pi^2}. \quad (\text{A.4})$$

For the imaginary part we find:

$$\text{Im } U(q^0, q, \Delta, \rho) = \begin{cases} \text{Im } \bar{U}(q^0 - \Delta, q, \rho) & \text{for } q^0 > \Delta \\ 0 & \text{for } q^0 < \Delta \end{cases} \quad (\text{A.5})$$

where

$$\text{Im } \bar{U}(q^0, q, \rho) = -\frac{3}{4}\pi\rho \frac{M}{qk_F} \left[ (1 - z^2)\theta(1 - |z|) - (1 - z'^2)\theta(1 - |z'|) \right] \frac{q^0}{|q^0|}, \quad (\text{A.6})$$

with

$$z = \frac{M}{qk_F} \left( q^0 - \frac{q^2}{2M} \right), \quad z' = \frac{M}{qk_F} \left( -q^0 - \frac{q^2}{2M} \right). \quad (\text{A.7})$$

## References

- [1] M. Alberg, E. M. Henley and L. Wilets, *Ann. of Phys.* **96** (1976) 43.
- [2] R. Brockmann, W. Weise and L. Tauscher *Nucl. Phys.* **A308** (1978) 365.
- [3] M. Mizoguchi, S. Hirenzaki and H. Toki, *Nucl. Phys.* **A567** (1994) 893.
- [4] C.J. Batty, *Nucl. Phys.* **A372** (1981) 418.
- [5] C. J. Batty, E. Friedman and A. Gal, *Phys. Rep.* **287** (1997) 385.
- [6] E. Friedman, A. Gal and C. J. Batty, *Nucl. Phys.* **A579** (1994) 518.
- [7] E. Friedman and A. Gal, *Phys. Lett.* **B459** (1999) 43.

- [8] S. Hirenzaki, Y. Okumura, H. Toki, E. Oset and A. Ramos, *Phys. Rev.* **C61** (2000) 055205.
- [9] A. Baca, C. García-Recio, J. Nieves *Nucl. Phys.* **A673** (2000) 335.
- [10] V. Koch, *Phys. Lett.* **B337** (1994) 7.
- [11] T. Waas, N. Kaiser and W. Weise, *Phys. Lett.* **B365** (1996) 12; **B379** (1996) 34; T. Waas and W. Weise, *Nucl. Phys.* **A625** (1997) 287.
- [12] M. Lutz, *Phys. Lett.* **B426** (1998) 12.
- [13] A. Ramos and E. Oset, *Nucl. Phys.* **A671** (2000) 481.
- [14] D.B. Kaplan and A.E. Nelson, *Phys. Lett.* **B175** (1986) 57.
- [15] G.E. Brown, V. Thorsson, K. Kubodera and M. Rho, *Phys. Lett.* **B291** (1992) 335; G.Q. Li, C.H. Lee and G.E. Brown, *Nucl. Phys.* **A625** (1997) 372.
- [16] J.A. Pons, S. Reddy, P.J. Ellis, M. Prakash, and J.M. Lattimer, *Phys. Rev.* **C62** (2000) 035803; J.A. Pons, J.A. Miralles, M. Prakash and J.M. Lattimer, astro-ph/0008389.
- [17] W. Cassing, E.L. Bratkovskaya, U. Mosel, S. Teis and A. Sibirtsev, *Nucl. Phys.* **A614** (1997) 415; E.L. Bratkovskaya, W. Cassing and U. Mosel, *Nucl. Phys.* **A622** (1997) 593.
- [18] G.Q. Li, C.H. Lee and G.E. Brown, *Phys. Rev. Lett.* **79** (1997) 5214.
- [19] R. Barth et al., *Phys. Rev. Lett.* **78** (1997) 4007.
- [20] F. Laue et al., *Phys. Rev. Lett.* **82** (1999) 1640.
- [21] A.D. Martin, *Nucl. Phys.* **B179** (1981) 33.
- [22] P.B. Siegel and B. Saghai, *Phys. Rev.* **C52** (1995) 392.
- [23] N. Kaiser, P.B. Siegel and W. Weise, *Nucl. Phys.* **A594** (1995) 325; N. Kaiser, T. Waas and W. Weise, *Nucl. Phys.* **A612** (1997) 297;
- [24] E. Oset and A. Ramos, *Nucl. Phys.* **A635** (1998) 99.
- [25] J. Caro Ramón, N. Kaiser, S. Wetzell and W. Weise, *Nucl. Phys.* **A672** (2000) 249.
- [26] M. Ericson and T.E.O. Ericson, *Ann. Phys.* **36** (1966) 323.
- [27] R. Seki and K. Masutani, *Phys. Rev.* **C27** (1983) 2799.
- [28] J. Nieves, E. Oset and C. García-Recio, *Nucl. Phys.* **A554** (1993) 509.
- [29] C. García-Recio, L.L. Salcedo and E. Oset, *Phys. Rev.* **C39** (1989) 595.

- [30] M. Lutz and W. Florkowski, nucl-th/0004020; Acta Phys. Polon. B31 (2000) 2567.
- [31] J.P. Jeukenne, A. Lejeune and C. Mahaux, *Phys. Rep.* **25** (1976) 83
- [32] J. Nieves and E. Ruiz Arriola, hep-ph/0104307, to appear in Phys.Rev.D.
- [33] J.A. Oller, E. Oset and J.R. Peláez, *Phys. Rev.* **D59** (1999) 074001
- [34] R. D. Mattuck, A guide to Feynman diagrams in the many body problem, Dover, 1976.
- [35] A.L. Fetter and J.D. Walecka, Quantum Theory of many particle systems, McGraw-Hill, 1971.
- [36] G.E. Brown, Many-body problems, North-Holland, 1972.
- [37] E. Oset, D. Strottman, H. Toki and J. Navarro, *Phys. Rev.* **D48** (1993) 2395.
- [38] C.B. Dover, J. Hüfner and R.H. Lemmer, *Ann. Phys.* **66** (1971) 248
- [39] J. Hüfner and C. Mahaux, *Ann. Phys.* **73** (1972) 525
- [40] J. Hüfner, *Phys. Rep.* **21** (1975) 1
- [41] C. García-Recio, E. Oset and L.L. Salcedo, *Phys. Rev.* **C37** (1988) 194.
- [42] J. Gasser and H. Leutwyler, *Ann. Phys.* **158** (1984) 142; J. Gasser and H. Leutwyler, *Nucl. Phys.* **B250** (1985) 465, 517, 539; A. Pich, *Rep. Prog. Phys.* **58** (1995) 563; G. Ecker, *Prog. Part. Nucl. Phys.* **35** (1995) 1; U.G. Meissner, *Rep. Prog. Phys.* **56** (1993) 903.
- [43] F. Klingl, N. Kaiser and W. Weise, *Nucl. Phys.* **A624** (1997) 527; F. Klingl, T. Waas and W. Weise, *Phys. Lett.* **B431** (1998) 254
- [44] E. Oset and A. Ramos, *Nucl. Phys.* **A679** (2001) 616
- [45] G. Ecker, J. Gasser, A. Pich, E. de Rafael, *Nucl. Phys.* **B321** (1989) 311
- [46] J.A. Oller and E. Oset. *Phys. Rev.* **D60** (1999) 074023
- [47] C. Itzykson and B. Zuber, *Quantum Field Theory*, McGraw-Hill (1969) New York.
- [48] E. Oset and L. L. Salcedo, *J. of Comp. Phys.* **57** (1985) 361.
- [49] C.W. de Jager, H. de Vries and C. de Vries, *At. Data and Nucl. Data Tables* **14** (1974) 479; 36 (1987) 495.
- [50] J.W. Negele and D. Vautherin, *Phys. Rev.* **C11** (1975) 1031 and references therein.